Eur. Phys. J. D **34**, 23–27 (2005)
DOI: 10.1140/epjd/e2005-00106-9

THE EUROPEAN PHYSICAL JOURNAL D

Stability patterns of transition metal doped silver clusters: Dopant- and size-dependent electron delocalization

E. Janssens, S. Neukermans, X. Wang, N. Veldeman, R.E. Silverans, and P. Lievens[a]

Laboratorium voor Vaste-Stoffysica en Magnetisme, K.U.Leuven, Celestijnenlaan 200D, 3001 Leuven, Belgium

Received 6 September 2004
Published online 13 July 2005 –

Abstract. The stability of cationic silver clusters doped with a $3d$ transition metal atom (Sc, Ti, V, Cr, Mn, Ni, Cu) is investigated by mass spectrometric analysis of fragments resulting from high fluence irradiation of a cluster beam. The mass spectra show enhanced stabilities that correspond to closed shells of valence electrons. Dopant- and size-dependent delocalization of $4s$ and $3d$ electrons is discussed based on spherical shell model considerations. Contrary to doped gold clusters, no evidence was found for the existence of 2D electronic shell closures.

PACS. 36.40.Cg Electronic and magnetic properties of clusters – 36.40.Qv Stability and fragmentation of clusters

1 Introduction

The technological relevance of small coinage metal clusters has stimulated research strongly [1]. Nanoscale gold and silver systems serve as catalyst in some specific reactions or as building blocks in nanostructured materials [2–5]. Small silver clusters are of great interest for their optical properties [6,7]. Tiny particles of silver are used for photographic materials since they react chemically when exposed to light and etch a reflection of the image viewed [8].

The atomic electron configuration of silver features a filled $4d$ shell and a singly occupied $5s$ shell. The d band is buried well below the Fermi level, therefore some similarities between silver and alkali metal clusters can be expected. Size dependent properties of silver clusters indeed show a shell structure with closed electronic shells for systems containing 2, 8, 20, 40, 58, 92, ... valence s electrons [9–14], which indicates that the properties of silver clusters can be treated to first approximation within a simple metal cluster framework.

While in silver clusters the valence s electrons are itinerant, the characteristics of clusters of transition metals having an open d shell are determined by more localized bonds. Their valence s electrons play an essential role in the atom-atom bonding, but the influence of directional bonding by electrons from the partially filled d levels is not negligible. With structural, magnetic and catalytic properties strongly depending on size, transition metal clusters are considered to be attractive for a wide range of applications [15]. However, chemical bonding in these species still is not fully understood.

A study of transition metal doped coinage metal clusters provides an elegant way to investigate the interplay between free electrons and directional bonds in small clusters [16,17]. Investigating the role of heterogeneous bonding in mixed clusters will elucidate the fundamental effects responsible for the stability of metal clusters. In addition the influence of the host on the local magnetism of the dopant can be considered [16].

In this paper we report the production of bimetallic Ag_nX^+ ($n < 60$, X = Sc, Ti, V, Cr, Mn, Ni, Cu) clusters. The clusters are studied with time-of-flight mass spectrometry after laser fragmentation. Analysis of the mass spectra provides a correspondence between observed enhanced stabilities and closed shells of electrons. The discussion will be based on phenomenological shell model considerations and will emphasize element- and size-dependent magic numbers. The results also will be compared with recent investigations of transition metal doped gold clusters [17–21].

2 Bimetallic cluster production and laser fragmentation

The transition metal doped silver clusters are produced with a dual-target dual-laser vaporization source [22]. Two metal targets are vaporized by two independent pulsed (10 Hz) Nd:YAG lasers. Atom condensation of the different metal elements into clusters is initiated by introducing helium gas into the source. The source parameters (gas pressure, laser energies, time delays between the opening of the gas valve and the vaporization of the metal targets, and source geometry) are optimized to achieve

[a] e-mail: peter.lievens@fys.kuleuven.ac.be

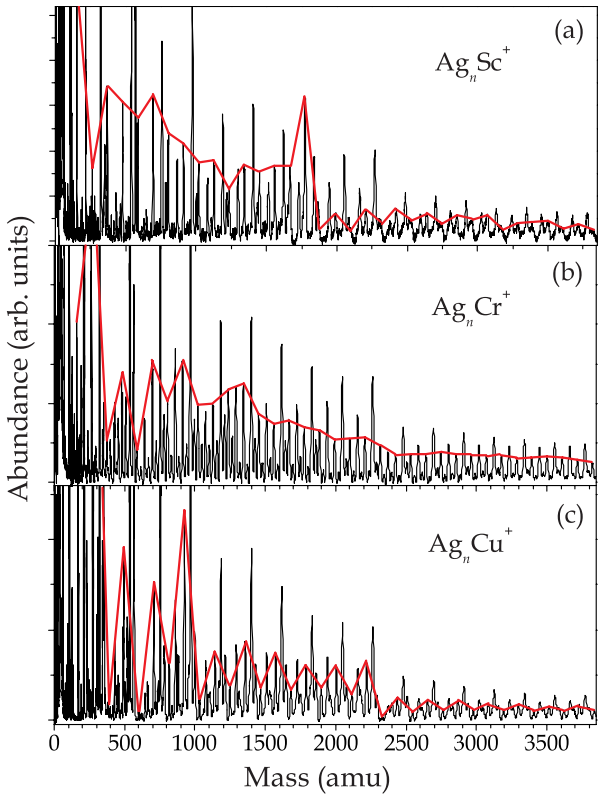

Fig. 1. Mass abundance spectra showing the cluster ion signals following photofragmentation for $Ag_nX_m^+$ ($n = 1$–35, $m = 0$–2) with X = Sc (a), Cr (b), and Cu (c). The peaks corresponding to Ag_nX^+ are connected by a solid line.

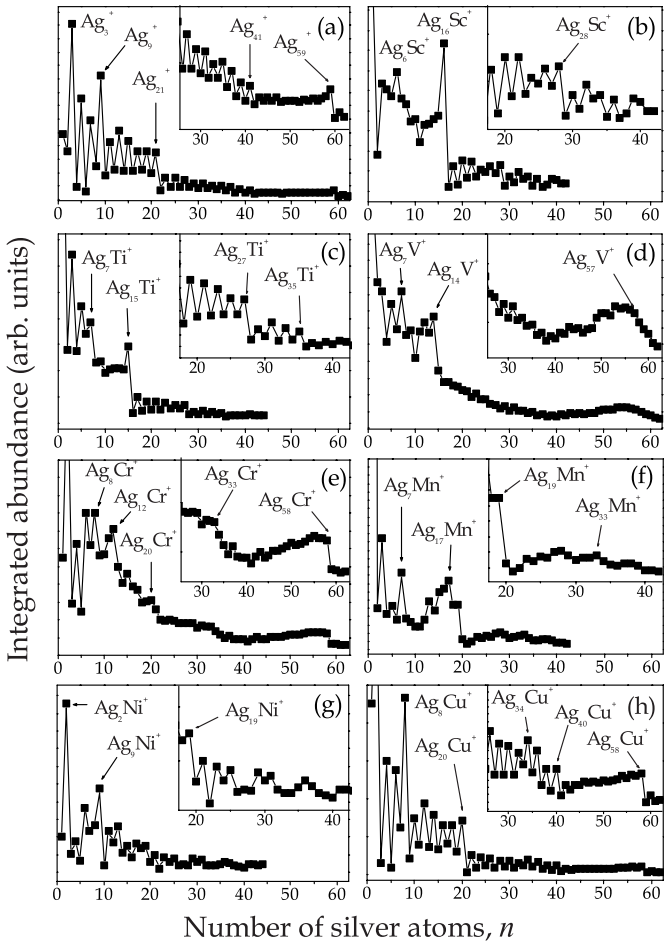

Fig. 2. Integrated cationic cluster abundances as a function of size for Ag_nX^+ with X = Ag (a), Sc (b), Ti (c), V (d), Cr (e), Mn (f), Ni (g), and Cu (h).

a maximal production of silver clusters containing a single dopant atom. The dopant target is vaporized typically 150 μs before the silver. Charged particles are electrostatically deflected out of the beam. The remaining neutral cluster beam is irradiated with high fluence laser light (>2 MW cm^{-2}, $\lambda = 193$ nm) generated by an excimer laser. The resulting photofragments reveal a size distribution with higher abundances for clusters with an enhanced stability.

The mass spectra for $Ag_nX_m^+$ (X = Sc, Cr, Cu) are shown in Figure 1. Each fragmentation spectrum is an average of at least ten independent measurements, where one measurement consists of 5000 production cycles. The stability patterns after photofragmentation are well reproducible and do not significantly depend on details of the initial cluster distribution nor on the exact fragmentation laser power. All mass spectra are baseline corrected for the non mass resolved ion signal. The most intense mass peaks correspond to pure Ag_n^+ clusters. On the right-hand side of the pure species, Ag_nX^+ peaks appear. They are connected by a solid line in Figure 1.

Peaks corresponding to larger sizes are broader because of the natural isotope distribution for silver (51.8% ^{107}Ag, 48.2% ^{109}Ag) and the limited resolution of our mass spectrometer ($M/\Delta M < 1000$). Peaks corresponding to $Ag_nX_2^+$ and Ag_{n+1}^+ partially overlap since the mass of the dopant atoms is about half the mass of a silver atom. Combined with the limited abundance of doubly doped species, the errors on the estimated $Ag_nX_2^+$ signals will be large. Therefore we will not deal with multiply doped silver clusters here.

3 Magic sizes for doped silver clusters

In Figure 2 the recorded abundances of singly doped Ag_nX^+ (X = Ag, Sc, Ti, V, Cr, Mn, Ni, Cu) clusters are presented. The plotted abundances equal the integrated areas of the corresponding mass peaks. The experimental spectra reveal an odd-even staggering (OES) and distinguished peaks or steps after specific cluster sizes (the magic sizes), that reflect a closed electronic shell structure. If an electron is added to these cluster sizes, it is forced to occupy the next (energetically less favorable) shell. The magic sizes are listed in Table 1, together with the proposed number of electrons contributed by the dopant atoms, n_v, to come to known magic numbers of electrons, n_e. Most of the observations qualitatively can be interpreted within a spherical shell model picture and

Table 1. Summary of the observed shell features. Intensity drops occur after Ag_nX^+. n_v is the proposed number of delocalized electrons stemming from the dopant. n_e denotes the total number of delocalized electrons in the magic Ag_nX^+ clusters. n_e values that do not correspond to known spherical shell closures are between brackets.

X	valence	n	n_v	n_e
Ag	$4d^{10}5s^1$	3, 9, 21, 41, 59	1	2, 8, 20, 40, 58
Sc	$3d^14s^2$	6, 16, 28	3	8, 18, (30)
Ti	$3d^24s^2$	7, 15, 27, 35	2, 4	8, 18, (30), (38)
V	$3d^34s^2$	7, 14, 57	2, 5	8, 18, 58
Cr	$3d^54s^1$	2, 8, 12, 20, 33, 58	1, 2	2, 8, (12), 20, 34, 58
Mn	$3d^54s^2$	1, 7, 17, 19, 33	2	2, 8, 18, 20, 34
Ni	$3d^84s^2$	2, 9, 19	0, 1	2, 8, 18
Cu	$3d^{10}4s^1$	2, 8, 20, 34, 40, 58	1	2, 8, 20, 34, 40, 58

provide information on the electronic behavior of the dopant atom in the cluster.

The patterns for pure Ag_n^+ clusters display an OES and steps in abundance after n = 3, 9, 21, 41, and 59. This confirms the presence of a shell structure that arises from the delocalization of the atomic valence 5s electrons in the silver clusters. Since cations have one conduction electron less than neutral clusters, the major features in the mass spectra are associated with the closing of electronic shells at total electron numbers 2, 8, 20, 40, and 58. This shell structure has been reported by different experimental studies [9–14].

For scandium and titanium doped silver clusters, there are striking peaks at $Ag_{16}Sc^+$ and $Ag_{15}Ti^+$ and steps after Ag_6Sc^+, $Ag_{28}Sc^+$, Ag_7Ti^+, $Ag_{27}Ti^+$, and $Ag_{35}Ti^+$. The distinct features correspond to the electron numbers 8, 18, 30, and 38 in case scandium delocalizes three and titanium two (Ag_7Ti^+) or four ($Ag_{15}Ti^+$, $Ag_{27}Ti^+$, and $Ag_{35}Ti^+$) electrons. Note that 30 and 38 are not known as a spherical magic number in pure silver clusters. There also is a clear OES for Ag_nSc^+ and Ag_nTi^+ in the $n > 15$ size range.

The pattern of vanadium doped silver clusters is rather smooth and only exhibits OES for small sizes ($n < 14$). Ag_nV^+ unveils local maxima at Ag_7V^+ and $Ag_{14}V^+$, and a smeared-out step around $Ag_{57}V^+$. These sizes can be linked with the magic numbers 8, 18, and 58 in case vanadium contributes two (in Ag_7V^+ and $Ag_{57}V^+$) or five (in $Ag_{14}V^+$) electrons to the cloud of itinerant electrons.

The observed steps after Ag_nCr^+ with n = 2, 8, 12, 20, and 58 are related to n_e = 2, 8, 12, 20, and 58 assuming that chromium donates one electron. Among these numbers, only 12 is not known as a spherical magic number. The step at $Ag_{33}Cr^+$ may be attributed to a shell closure for 34 electrons, if chromium provides two electrons in this cluster. Remark that the amplitude of the OES for Ag_nCr^+ is modest for all but the smallest sizes ($n < 10$).

The prominent intensity variations at Ag_1Mn^+, Ag_7Mn^+, $Ag_{17}Mn^+$, and weaker ones at $Ag_{19}Mn^+$ and $Ag_{33}Mn^+$ can be associated with n_e = 2, 8, 18, 20, and 34 if manganese contributes two electrons.

For nickel doped silver clusters, drops in abundance occur after Ag_2Ni^+, Ag_9Ni^+, and $Ag_{19}Ni^+$, in addition to an obvious OES. The magic sizes might correspond to the numbers 2, 8, and 18 in case nickel delocalizes one (for Ag_2Ni^+) or zero electrons (for Ag_9Ni^+ and $Ag_{19}Ni^+$). Note that the difference in the number of itinerant electrons contributed by nickel accords with the altering of the OES at $n = 8$. For $n < 8$ the maxima are at even n values, while for $n > 8$, the even n values correspond to minima in the stability pattern.

The stability pattern of Ag_nCu^+ is much the same as for pure Ag_{n+1}^+ clusters. A clear OES is present over the entire size range together with steps after Ag_nCu^+ with n = 2, 8, 20, 34, 40, and 58.

4 Dopant valence electron delocalization

Here an interpretation of the interaction of the transition metal electrons with the silver matrix is presented. We focus on three points: (i) the relation between n_v and the valences of the dopant atoms, (ii) the size dependent electron delocalization, and (iii) the appearance of new magic numbers.

(i) A comparison between the dopant valences and n_v, both given in Table 1, yields the following results. The magic character of Ag_nSc^+ (n = 6, 16), $Ag_{15}Ti^+$, and $Ag_{14}V^+$ agrees with spherical magic numbers if as well the dopant 4s as 3d electrons contribute to the cloud of itinerant electrons. Ag_7Ti^+, Ag_7V^+, $Ag_{57}V^+$, and the magic Ag_nX^+ clusters doped with the heavier elements (X = Cr, Mn, Ni, and Cu) correspond to known magic numbers, if only the 4s electrons of the dopant atoms are itinerant. The misfit between the nickel $3d^84s^2$ atomic configuration and n_v = 0,1 as well as the size dependent behavior of chromium are treated in (ii). The dissimilarity between the light (Sc) and the heavier (Cr, Mn, Ni, Cu) dopants can be accounted for by differences in the spatial extent of the occupied d orbitals. The large size of the d electron wave functions of metals at the beginning of the 3d series [16] results in strong hybridization with the Ag electron orbitals. Ag_nTi^+ and Ag_nV^+ form the intermediate range. Here, it is believed that the dopant 3d electrons only behave itinerant if the hybridization with the host 5s electrons is strong.

(ii) Only the Ag_nX^+ (X = Sc, Mn, and Cu) patterns could be explained assuming a fixed number of electrons delocalized by the dopant atom (see Tab. 1). The magic sizes found for other Ag_nX^+ (X = Ti, V, Cr, Ni) clusters correspond to known magic numbers if the delocalization behavior of the dopant atoms depends on the cluster size. Ag_nTi^+ and Ag_nV^+ were discussed in (i). For Ag_nCr^+ and Ag_nNi^+ the size dependence might be related to the small energy difference between the transition metal atom $3d^x4s^2$ and $3d^{x+1}4s^1$ (or $3d^{x+2}4s^0$ for Ni) configurations. The preferred valence electron configuration depends on details of the interaction with the host, such as the cluster size, the kind of host, and the coordination of the dopant [17]. In Ag_nX^+ with X = Sc, Mn, and Cu, a size independent number of itinerant electrons is contributed by the dopant atom, in agreement with the larger $3d^x4s^2 - 3d^{x+1}4s^1$ energy difference.

(iii) While 18 is not seen as a magic number in the stability pattern of pure silver clusters, it correlates with the most striking feature in the Ag_nX^+ (X = Sc, Ti, V, Mn) patterns. The manifestation of a shell closure for 18 electrons can be related to a modification of the potential felt by the valence electrons by introducing a dopant atom. If the dopant is assumed to be located in the center of the cluster, a central hump in the effective potential (the dopant has a lower electronegativity than silver) causes an upward shift of the (shell model) $2s$ energy level, which makes the magic number 20 disappear, in favor of 18. A similar explanation has been used to explain the enhancement of the magic number 18 in the stability patterns of doped gold clusters [17,18,23].

The disappearance of the magic number 40 and the appearance of $n_e = 34$ in Ag_nX^+ (X = Cr, Mn, Cu) might be related with $s-d$ hybridization between dopant $3d$ and host $5s$ electrons in the doped systems. An enhanced $s-d$ hybridization modifies the mean field potential and causes the magic number 34 to be present. This also can be the reason why Au_{35}^+ is a magic size and not Ag_{35}^+.

Other magic numbers only appear for specific dopants: 30 ($Ag_{28}Sc^+$ and $Ag_{27}Ti^+$), 38 ($Ag_{35}Ti^+$), and 12 ($Ag_{12}Cr^+$). Probably these magic numbers can be formed by subshell closure and/or shell inversions related to a deformed geometry. However, no conclusive explanation can be given at this point; more information from quantum chemical calculations on the electronic structure is required.

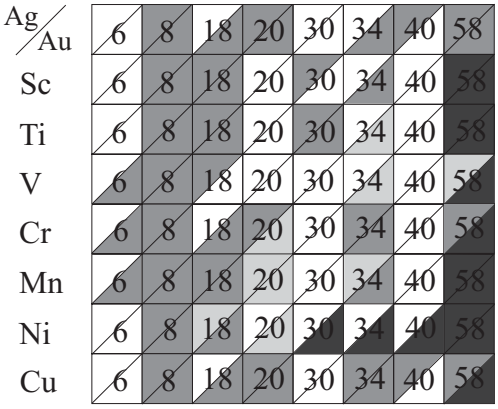

Fig. 3. Representation of the observed magic numbers for Ag_nX^+ and Au_nX^+ clusters. The first row lists the results for pure silver and gold, the other rows are for the doped species. Doped silver is indicated by the upper-left triangles, doped gold by the lower-right triangles. Electron numbers shaded in grey are observed as magic, the ones in light grey reveal a slightly enhanced stability. For numbers shaded in dark grey, no experimental results are recorded.

5 Comparison with doped gold clusters

While the magic numbers observed in Ag_n and Au_n are alike [9] (except for $34 \leftrightarrow 40$), there are important differences in the degree of $s-d$ hybridization leading to different ground state geometries [1]. The $s-d$ hybridization is small in silver, because its d band locates well below the Fermi level [10]. The chemistry of silver clusters is basically dominated by the s electrons, there are no directional bonds [24]. The well-established $s-d$ hybridization in gold leads to rather large s and d bandwidths, and to more directional and stronger bonds compared to silver clusters of the same size [25]. An additional consequence is the propensity to favor planar geometries, since $d-d$ bonds are optimal in a 2D structure [25,26].

Photofragmentation studies of Au_nX^+ (X = Sc, Ti, V, Cr, Mn, Fe, Co, Cu, and Zn) clusters revealed electronic shell structures and dopant induced changes in the shell sequence [17–20]. The magic numbers found for Au_nX^+ are presented schematically in Figure 3 and compared with the observations for Ag_nX^+.

The photofragmentation patterns of doped gold and silver clusters uncover several similarities. Also in a gold cluster, the lightest $3d$ elements (Sc, Ti) delocalize their $4s$ and $3d$ electrons, while for the heavier dopants (Cr, Mn, Fe, Co, Ni) only the $4s$ electrons become itinerant [17,19]. In both types of host, clusters with 18 valence electrons are remarkably stable, in particular $Au_{16}Sc^+$, $Ag_{16}Sc^+$, $Au_{15}Ti^+$, $Ag_{15}Ti^+$, and $Ag_{14}V^+$. A (new) magic number for 30 delocalized electrons appears both in $Au_{27}Ti^+$ and $Ag_{27}Ti^+$. Doping with copper has no big influence on the electronic shell structure of a gold or a silver cluster. Probably the mean field potential experienced by the electrons is only slightly modified when substituting a silver or a gold atom by a copper atom [17,18].

However, there is an important difference between the stability patterns of doped silver and doped gold clusters. Au_5X^+ (X = V, Cr, Mn, Fe, Co, and Zn) species showed up as very stable in the Au_nX^+ fragmentation spectra [17]. These six electron species are magic because of their 2D structure in combination with six being a magic number for 2D systems [20,21]. There is no enhanced intensity for six electron species in the Ag_nX^+ fragmentation spectra. Silver clusters are known to become three dimensional for smaller cluster sizes [24,25], in agreement with the absence of 2D magic numbers in our experiments.

6 Conclusion

Stability patterns of Ag_nX^+ (X = Sc, Ti, V, Cr, Mn, Ni, Cu) reflect an electronic shell structure with dopant dependent magic numbers. The open $3d$ shell transition metal dopant is considered to contribute its $4s$ electrons (for Cr up to Ni) or its $3d$ and $4s$ electrons (Sc and selected sizes for Ti and V) to a cloud of itinerant electrons. The size dependent electron delocalization is attributed to the small energy difference between $3d^x4s^2$ and $3d^{x+1}4s^1$ atomic configurations of the dopant atoms. Contrary to doped gold clusters, no evidence was found for the existence of 2D electronic shell closures in doped silver clusters.

This work is supported by the Fund for Scientific Research – Flanders (FWO), the K.U. Leuven Research Fund (GOA/2004/02 program) and the Belgian Interuniversity Poles of Attraction (IAP V/01 program). E.J. and S.N. are postdoctoral researchers of the FWO.

References

1. P. Pyykkö, Angew. Chem. Int. Ed. **43**, 4412 (2004)
2. M. Haruta, M. Daté, Appl. Catal. A: Gen. **222**, 427 (2001)
3. L.D. Socaciu, J. Hagen, J. Le Roux, D. Popolan, T.M. Bernhardt, L. Wöste, S. Vajda, J. Chem. Phys. **120**, 2078 (2004)
4. Y.D. Kim, G. Ganteför, Chem. Phys. Lett. **383**, 80 (2004)
5. V. Bonačić-Koutecký, J. Burda, R. Mitrić, M.F. Ge, G. Zampella, P. Fantucci, J. Chem. Phys. **117**, 3120 (2002)
6. S.A. Nepijko, D.N. Ievlev, W. Schulze, Eur. Phys. J. D **24**, 115 (2003)
7. M. Gaudry, E. Cottancin, M. Pellarin, J. Lermé, L. Arnaud, J.R. Huntzinger, J.L. Vialle, M. Broyer, J.L. Rousset, M. Treilleux, P. Mélinon, Phys. Rev. B **67**, 155409 (2003)
8. P. Fayet, F. Granzer, G. Hegenbart, E. Moisar, B. Pischel, L. Wöste, Phys. Rev. Lett. **55**, 3002 (1985)
9. I. Katakuse, T. Ichihara, Y. Fujita, T. Matsuo, T. Sakurai, H. Matsuda, Int. J. Mass Spectrom. Ion Proc. **67**, 229 (1985)
10. K.J. Taylor, C.L. Pettiette-Hall, O. Cheshnovsky, R.E. Smalley, J. Chem. Phys. **96**, 3319 (1992)
11. C. Jackschath, I. Rabin, W. Schulze, Z. Phys. D **22**, 517 (1992)
12. G. Alameddin, J. Hunter, D. Cameron, M.M. Kappes, Chem. Phys. Lett. **192**, 122 (1992)
13. S. Krückeberg, G. Dietrich, K. Lützenkirchen, L. Schweikhard, C. Walther, J. Ziegler, J. Chem. Phys. **110**, 7216 (1999)
14. M. Schmidt, Ph. Cahuzac, C. Bréchignac, H.P. Cheng, J. Chem. Phys. **118**, 10956 (2003)
15. J.A. Alonso, Chem. Rev. **100**, 637 (2000)
16. Q. Sun, Q. Wang, J.Z. Yu, Z.Q. Li, J.T. Wang, Y. Kawazoe, J. Phys. I **7**, 1233 (1997)
17. S. Neukermans, E. Janssens, H. Tanaka, R.E. Silverans, P. Lievens, Phys. Rev. Lett. **90**, 33401 (2003)
18. W. Bouwen, F. Vanhoutte, F. Despa, S. Bouckaert, S. Neukermans, L.T. Kuhn, H. Weidele, P. Lievens, R.E. Silverans, Chem. Phys. Lett. **314**, 227 (1999)
19. E. Janssens, H. Tanaka, S. Neukermans, R.E. Silverans, P. Lievens, Phys. Rev. B **69**, 085402 (2004)
20. E. Janssens, H. Tanaka, S. Neukermans, R.E. Silverans, P. Lievens, New J. Phys. **5**, 46 (2003)
21. H. Tanaka, S. Neukermans, E. Janssens, R.E. Silverans, P. Lievens, J. Am. Chem. Soc. **125**, 2862 (2003)
22. W. Bouwen, P. Thoen, F. Vanhoutte, S. Boeckaert, F. Despa, H. Weidele, R.E. Silverans, P. Lievens, Rev. Sci. Instrum. **71**, 54 (2000)
23. M. Heinebrodt, N. Malinowski, F. Tast, W. Branz, I.M.L. Billas, T.P. Martin, J. Chem. Phys. **110**, 9915 (1999)
24. P. Weis, T. Bierweiler, S. Gilb, M.M. Kappes, Chem. Phys. Lett. **355**, 355 (2002)
25. H. Häkkinen, M. Moseler, U. Landman, Phys. Rev. Lett. **89**, 033401 (2002)
26. F. Furche, R. Ahlrichs, P. Weis, C. Jacob, S. Gilb, T. Bierweiler, M.M. Kappes, J. Chem. Phys. **117**, 6982 (2002)